

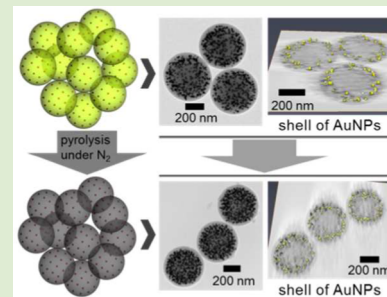
## Polymer and Carbon Spheres with an Embedded Shell of Plasmonic Gold Nanoparticles

Mostafa K. Khan and Mark J. MacLachlan\*

Department of Chemistry, University of British Columbia, 2036 Main Mall, Vancouver, British Columbia V6T 1Z1, Canada

### S Supporting Information

**ABSTRACT:** Gold nanoparticle (AuNP)/resin nanosphere composites have been prepared in a novel process where the resin functions as both the host and reducing agent. Electron tomography showed that the AuNPs are organized into a concentric shell fully embedded in the resin nanospheres. Pyrolysis of the composite spheres afforded microporous N-doped carbon nanospheres with a pseudoshell of embedded AuNPs. These new composites with uncapped plasmonic nanoparticles have excellent potential for biomedical, catalysis, energy storage, and sensing applications.



Gold nanoparticles (AuNPs) have unique optical properties<sup>1</sup> and reactivity that make them useful for bioimaging,<sup>2</sup> cancer therapy,<sup>3</sup> sensing,<sup>4</sup> catalysis,<sup>5</sup> and other applications.<sup>6</sup> Incorporating AuNPs into polymer nanospheres is attractive for developing biocompatible nanomaterials and plasmonic photonic crystals.<sup>6</sup> Methods to form these structures typically place the AuNPs at either the core or the periphery of the nanospheres<sup>7</sup> and frequently suffer from complicated syntheses or poor adhesion between the polymer sphere and the nanoparticles.

Hybrid AuNP/polymer spheres with the AuNPs at the center can be made by using AuNPs to seed the growth of a resin.<sup>8</sup> However, thick polymer shells diminish the impact and accessibility to the AuNP core. Alternatively, hybrid AuNP/polymer spheres may be made where the AuNPs are localized on the surface by either attaching or adsorbing preformed AuNPs to the polymer spheres.<sup>9</sup> These suffer from rough surfaces and often poor adhesion between the AuNPs and the resin sphere. AuNPs can also be synthesized *in situ* in resin spheres by using a secondary reducing agent and allowing the AuNPs to adsorb on the surface.<sup>10</sup> Uncontrolled growth results in polydisperse AuNPs that tend to aggregate and unevenly adsorb on the surface of the spheres. Moreover, in this case, AuNPs are prone to disintegration due to weak interaction between them and colloidal resin surfaces, affecting the longevity and reusability of the materials. Despite the substantial developments in this field, there is a need to create additional architectures that will allow further exploration of these fascinating nanomaterials.

Here we report a new type of hybrid nanomaterial comprised of nearly monodisperse resin spheres with a fully embedded pseudoshell of gold nanoparticles. These structures are formed by a surprising, straightforward matrix-assisted reduction of gold(III) ions in the resin spheres. Pyrolysis of these hybrid nanospheres in an inert atmosphere produced nitrogen-doped

carbon/AuNP composite spheres with complete retention of the original morphology. Our findings may lead to new materials that can be applied to biomedical applications, sensing, energy storage, and catalysis.

In this work, nearly monodisperse colloidal resin nanospheres were prepared at 30 °C from 3-aminophenol and formaldehyde in water/ethanol (Figure 1),<sup>11</sup> and they were purified by repeated centrifugation and sonication.

Nanosphere diameters were varied by changing the concentration of the resin precursors in the experiments to obtain samples RNS1 (diameter = 541 ± 29 nm), RNS2 (307 ± 13 nm), RNS3 (210 ± 10 nm), and RNS4 (118 ± 3 nm). Transmission electron microscopy (TEM) and scanning electron microscopy (SEM) images (Figure S1) showed that the spheres have smooth, uniform surfaces, and less than ~5% variance in their diameters.

FTIR spectra (Figure S2) of as-synthesized resin spheres show broad bands attributed to O–H and N–H stretching at 3200–3600 cm<sup>-1</sup>. Specifically, bands at ~3228 and ~3365 cm<sup>-1</sup> are assigned to O–H and N–H stretching modes, respectively. The O–H stretching bands diminish with respect to the N–H stretching band when the spheres are cured at 100 °C for 24 h, indicating enhanced cross-linking via condensation of phenolic and hydroxymethyl OH groups. Differential scanning calorimetry of RNS1 (Figure S3) shows an endothermic peak at 181 °C that arises from the polycondensation (cross-linking) of the resin spheres. Together, these observations indicate that as-synthesized resin spheres are only lightly cross-linked, with a high density of hydroxymethyl groups (Figure 1). Consequently, the resin spheres are porous and swell in water.

Received: October 17, 2015

Accepted: November 16, 2015

Published: November 19, 2015

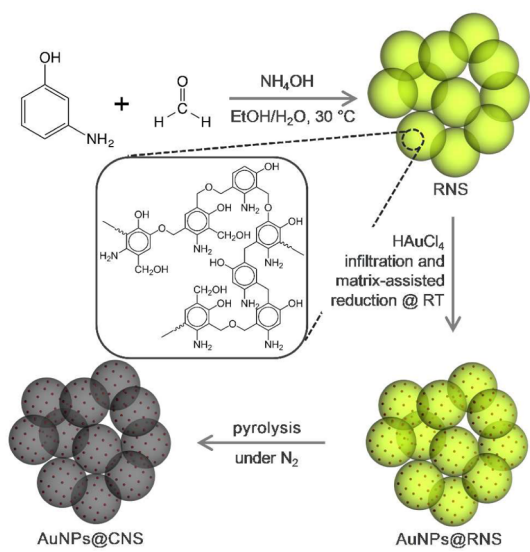


**Figure 1.** Synthesis of resin nanospheres (RNS), gold-containing resin nanospheres (AuNPs@RNS), and carbonized resin nanospheres (AuNPs@CNS).

As benzyl alcohols are known reducing agents for Au<sup>3+</sup>,<sup>12</sup> we hypothesized that HAuCl<sub>4(aq)</sub> could infiltrate the resin spheres and form AuNPs without the need for an external reducing

agent. For our work, it was essential to remove all unreacted resin precursors that were trapped in the spheres and could leach out during the gold deposition (see SI and Figures S4 and S5). As well, adding HAuCl<sub>4</sub> directly to the resin sphere preparation gave a dirty, complex product (Figure S6).

When HAuCl<sub>4</sub> was added to each of the purified resin spheres RNS1–RNS4, the samples rapidly changed from off-white/yellow to red (Figure S7), giving products AuNPs@RNS1–4, respectively. SEM images (Figure 2a–d) of AuNPs@RNS1–4 clearly show the gold nanoparticles distributed within the resin spheres. The smooth surface of AuNPs@RNS1 reveals that AuNPs are dispersed inside the resin spheres, not deposited on the surface (Figure S8). TEM images (Figure 2e–h; Figure S9) further confirm that AuNPs are formed inside the resin spheres and there are no AuNPs on the surface. We did not see any significant change in nanosphere size after addition of gold.

To obtain further insight into the structures of the composite nanospheres, AuNPs@RNS1–4 were investigated by electron tomography. Rendered 3D tomograms (Figures 3 and S10–12; Movies S1–8) verified that AuNPs were formed inside the resin spheres and remained well-dispersed in the resin matrix. Remarkably, the AuNPs are not homogeneously dispersed throughout the resin sphere, as we expected, but instead form a ~75 nm thick shell ~195 nm from the center (Figure S13). Cross sections of AuNPs@RNS1 (Figure 3) clearly show that

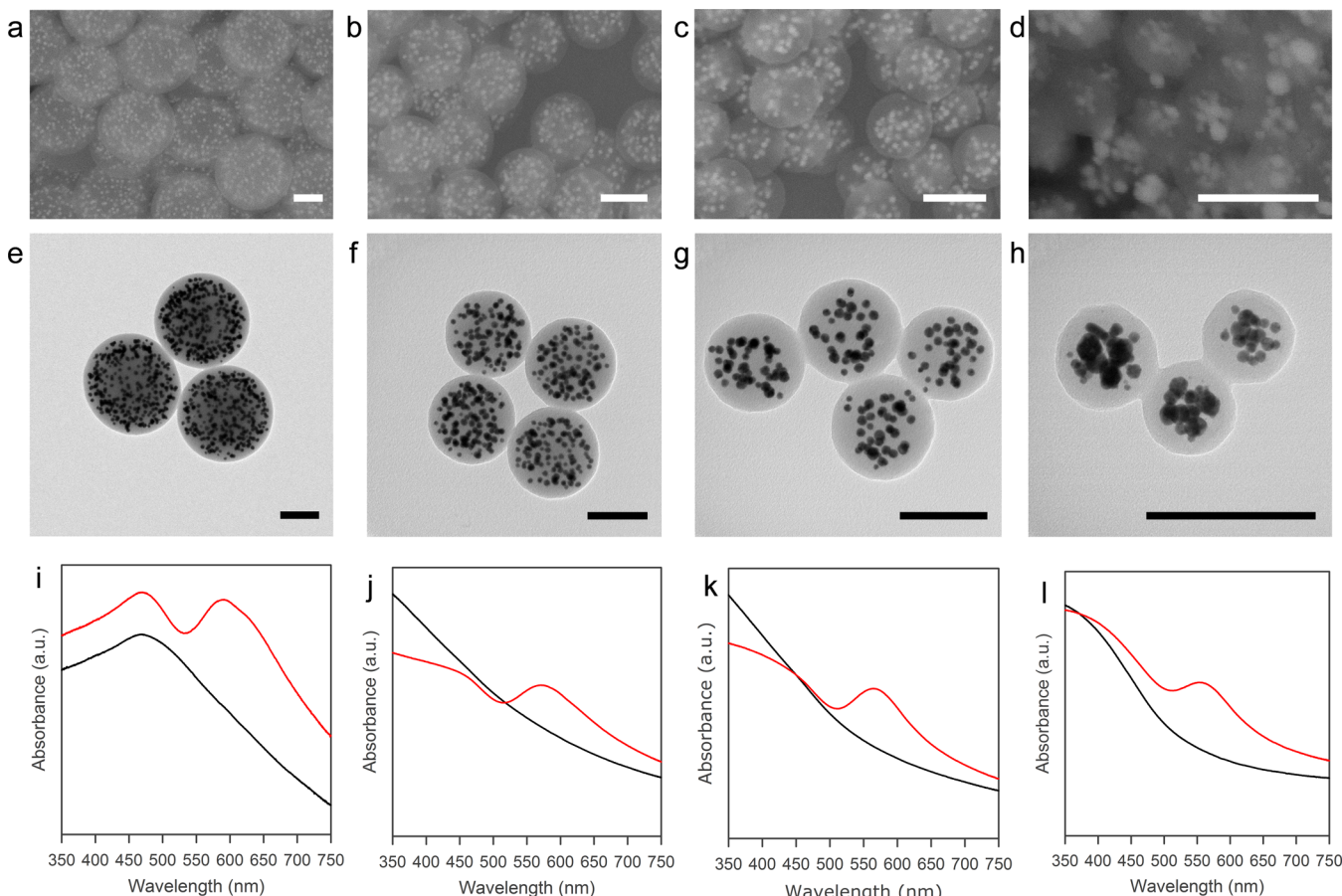


**Figure 2.** SEM images taken with back scattered electron (BSE) detector (top, a–d), TEM images (middle, e–h), and UV–vis spectra (bottom, i–l) of AuNPs@RNS1 (a, e, i), AuNPs@RNS2 (b, f, j), AuNPs@RNS3 (c, g, k), and AuNPs@RNS4 (d, h, l). Each column shows the SEM image, TEM image, and UV–vis spectra of a particular AuNP@RNS sample. Scale bars, 200 nm. Black and red traces in (i–l) represent the UV–vis spectra of the corresponding RNS and AuNPs@RNS samples, respectively.

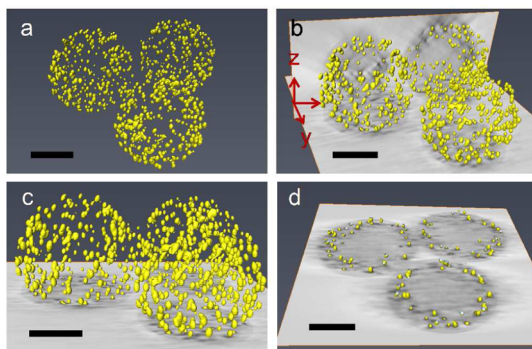


**Figure 3.** (a, b) Rendered 3D tomogram of AuNPs@RNS1 showing the pseudoshells of AuNPs embedded within the resin nanospheres. (c) Pseudoshell of AuNPs on *xy* plane shown from a different viewing angle. (d) View of the cross-section showing the absence of AuNPs at the core of the resin nanospheres. Scale bars, 200 nm.

there are no AuNPs at the core of the resin spheres. AuNPs are mostly spherical in shape, with an average diameter of  $18 \pm 3$  nm calculated from TEM images.

AuNPs formed in RNS2 and RNS3 (AuNPs@RNS2, AuNPs@RNS3) are also distributed in a spherical shell (**Figures S10 and 11**). In contrast, TEM images and electron tomograms of AuNPs@RNS4 (**Figures 2f and S12**) show that AuNPs are located throughout the resin spheres. These observations suggest that HAuCl<sub>4</sub> can only penetrate a finite depth into the resin spheres before it is reduced to a nanoparticle by the resin. When the Au<sup>3+</sup> diffuses into the large resin nanospheres and undergoes reduction, the AuNPs formed get trapped in a concentric pseudoshell. The penetration depth may be dictated by the denser cross-linking at the center of the resin nanosphere that prevents diffusion of the AuNPs, or by anchoring of the AuNPs when they reach a critical size. On the other hand, AuNPs formed in resin nanospheres smaller than  $\sim 200$  nm are distributed throughout the resin spheres. Thus, the size-tunability of the resin spheres provides a unique way to control the morphology of the nanocomposite materials.

AuNPs show a localized surface plasmon resonance (SPR) that arises from collective oscillation of conduction electrons. UV-visible spectra of the AuNPs@RNS1–4 dispersed in water all show bands at 550–600 nm (**Figure 2i–l**) arising from the SPR of AuNPs.<sup>13</sup> (In the case of AuNPs@RNS1, the polymer spheres themselves scatter light and show a peak at  $\sim 500$  nm; this is also evident in the polymer spheres RNS1, **Figure 2i**.) Powder X-ray diffraction (PXRD) of select samples showed that the AuNPs are crystalline gold (**Figure S14**). These data agree with the TEM results, which clearly show discrete AuNPs in each sample.

We investigated the effect of concentration of HAuCl<sub>4</sub> on the morphology of the composite nanospheres. Three samples were prepared by dispersing equal amounts of RNS1 in 0.1, 0.5, and 1.0 mM aqueous solution of HAuCl<sub>4</sub> and stirring at room temperature for 2 h (AuNPs@RNS1–0.1, AuNPs@RNS1–0.5, and AuNPs@RNS1–1.0, respectively). TEM images (**Figure S15**) show that sample AuNPs@RNS1–0.1 has completely different morphology than the other two samples, with only very small AuNPs localized on the surface of the resin nanospheres. In contrast, AuNPs@RNS1–0.5 and AuNPs@RNS1–1.0 have substantially larger AuNPs, and all are inside the resin nanospheres. Moreover, it is clearly seen that, with

increasing Au<sup>3+</sup> concentration, more AuNPs are incorporated into the resin spheres.

We also investigated the effect of reaction time on the morphology of the composite nanospheres prepared with 1.0 mM HAuCl<sub>4</sub>. TEM images of samples prepared for different times (10–120 min) are shown in **Figure S16**. It is noteworthy that there is no significant effect of reaction time on morphology of the resulting composites. In our procedure, the gold precursor is reduced within 10 min without any secondary reducing agent, and the nanoparticles formed are rapidly trapped in the resin. This is a straightforward, high-throughput process in which composite nanomaterials comprising of resin spheres with a pseudoshell of metal nanoparticles can be synthesized at room temperature.

Considering the growing interest in microporous carbon spheres,<sup>14</sup> we wondered whether the gold-containing resin nanospheres could be converted to carbon materials, maintaining the hierarchical structure. Thermogravimetric analysis of AuNPs@RNS1 showed a different degradation profile from RNS1 and yielded  $\sim 66$  wt % char at 600 °C (**Figure S17**) compared with 55 wt % for RNS1. Bulk pyrolysis of RNS1 and AuNPs@RNS1 at 600 °C under nitrogen afforded N-doped carbon nanospheres (CNS1) and AuNP/N-doped carbon nanospheres (AuNPs@CNS1), respectively (**Figures 4a,b and S18**). FTIR spectra of CNS1 and AuNPs@CNS1

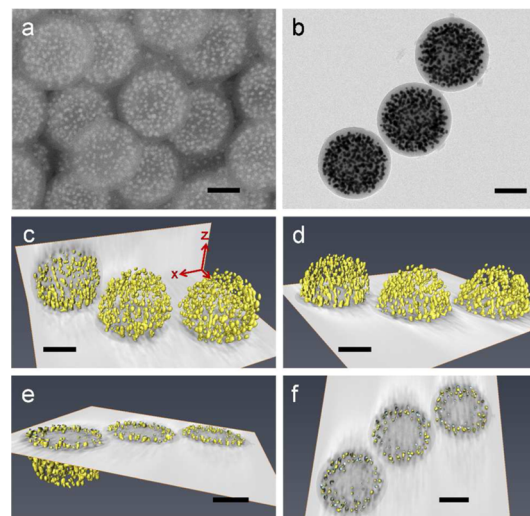


**Figure 4.** (a) SEM image, captured with BSE detector, and (b) TEM image of AuNPs@CNS1. (c) Rendered 3D tomogram showing the pseudoshells comprising AuNPs that are embedded within the carbon nanospheres. (d) Pseudoshell of AuNPs on *xy* plane shown from a different viewing angle. (e) and (f) View of the cross-section from two different angles showing the absence of AuNPs at the carbon nanospheres' cores. Scale bars, 200 nm.

samples (**Figure S19**) are nearly identical, indicating that the presence of AuNPs does not significantly alter the chemical nature of the resulting carbon materials. Absorption bands at  $\sim 1550$  and  $\sim 1200$  cm<sup>-1</sup>, with a shoulder at 1246 cm<sup>-1</sup>, are attributed to C=C modes and mixed C=N modes of nitrogen-doped carbons.<sup>15</sup> Most of the absorption bands observed in IR spectra of as-synthesized resin spheres (**Figure S2**) disappear after carbonization. Elemental analysis (**Table S2**) shows that CNS1 contains over 78% carbon with low hydrogen content (2.36%). As expected, the sample contains substantial amounts of nitrogen (8.2%) derived from the

aminophenol precursor. In contrast, ~50% less C, N, and H were measured in AuNPs@CNS1 that can be attributed to very high loading of gold in the composite carbon spheres. N<sub>2</sub> adsorption analysis of CNS1 (Figure S20) shows the carbon spheres are microporous with Brunauer–Emmett–Teller (BET) surface area of ~275 m<sup>2</sup>/g and pore volume of 0.18 cm<sup>3</sup>/g. Barrett–Joyner–Halenda (BJH) pore size analysis shows that the pores are less than ~2 nm in diameter. Composite AuNPs@CNS1 is also microporous, but has a lower BET surface area (~105 m<sup>2</sup>/g) and pore volume (0.09 cm<sup>3</sup>/g) owing to the pore-filling and contribution to the sample density by AuNPs.

Electron microscopy of AuNPs@CNS1 proved that the spherical morphology of the particles was completely preserved (Figure 4a,b). Rendered 3D tomograms (Figure 4c–f and Movies S9 and 10) clearly show that the shell of AuNPs remains inside the carbon nanospheres, similar to the corresponding composite resin spheres. Electron tomography of the cross-section of the resin spheres (Figure 4c–f) confirms that there are no AuNPs at the core of the carbon spheres. Overall, AuNPs@CNS1 retains the same morphology of the corresponding AuNPs@RNS1 from which it was derived.

Gold nanoparticle-loaded carbon nanospheres were further investigated with PXRD and Raman spectroscopy. PXRD of CNS1 (Figure S21) shows two broad peaks around 21° and 44° 2θ attributed to the diffraction from amorphous carbon. An additional peak at 26.6° 2θ assigned to the reflection arising from graphitic carbon indicates that partial graphitization of the resin spheres has occurred during carbonization. PXRD of AuNPs@CNS1 (Figure S21) shows a similar diffraction pattern with additional reflection peaks arising from AuNPs. Notably, the broad peaks corresponding to the amorphous and graphitic carbons are still present, but their intensity is much lower than the peaks attributed to nanocrystalline gold. Raman spectroscopy of CNS1 (Figure S22) shows two low-intensity peaks at 1340 cm<sup>-1</sup> (D-band associated with disordered (amorphous) carbon) and 1565 cm<sup>-1</sup> (G-band associated with graphitic carbon). The G band is enhanced relative to the D band in AuNPs@CNS1 when compared to CNS1, consistent with enhanced graphitization in the AuNP-containing sample. We also noted that the intensity of the peaks in spectrum of AuNPs@CNS1 are enhanced by approximately 20× compared to those for CNS1. The greatly improved intensity and signal-to-noise ratio can be attributed to a surface-enhanced Raman scattering (SERS) effect of gold-loaded carbon nanospheres.<sup>16</sup> Since the spherical shape and uniform size of the AuNPs@CNS1 allow them to be easily packed and organized into an array, these materials can be applied as substrates in fabricating nanodevices for SERS-based sensing applications.

We have demonstrated, for the first time, a straightforward route to polymer nanospheres with a concentric pseudoshell of dispersed AuNPs. By purifying the resin nanospheres carefully, they can function as reductant for HAuCl<sub>4</sub> within the resin spheres, without formation of NPs on the surface. The diameter of the AuNP shell can be controlled by changing the size of the resin spheres. Furthermore, the AuNP/resin composite spheres can be pyrolyzed to obtain novel N-doped carbon spheres with a concentric shell of AuNPs. Considering the diversity of resins and metal precursors available, the convenient and scalable methods described in this paper are anticipated to give new materials with intriguing architectures. These plasmonic composite materials may be applied in biomedical applications, sensing, energy storage, and heterogeneous catalysis.

## ASSOCIATED CONTENT

### S Supporting Information

Electron tomography videos and supporting electron micrographs. The Supporting Information is available free of charge on the ACS Publications website at DOI: 10.1021/acsmacrolett.5b00742.

Synthesis details and supporting spectra (PDF).

(MPG)

## AUTHOR INFORMATION

### Corresponding Author

\*E-mail: mmaclach@chem.ubc.ca.

### Notes

The authors declare no competing financial interest.

## ACKNOWLEDGMENTS

This work was supported by NSERC (Discovery Grant). We thank Bradford Ross of UBC Bioimaging Facility for assistance in electron tomography and Najmeh Tavassoli for help in Raman spectroscopy.

## REFERENCES

- (a) Lee, K.; Cui, Y.; Lee, L. P.; Irudayaraj, J. *Nat. Nanotechnol.* **2014**, *9*, 474. (b) Kelly, P. M.; Åberg, C.; Polo, E.; O'Connell, A.; Cookman, J.; Fallon, J.; Krpetić, Ž.; Dawson, K. A. *Nat. Nanotechnol.* **2015**, *10*, 472.
- (a) Dreaden, E. C.; Mackey, M. A.; Huang, X.; Kang, B.; El-Sayed, M. A. *Chem. Soc. Rev.* **2011**, *40*, 3391. (b) Kim, C.; Agasti, S. S.; Zhu, Z.; Isaacs, L.; Rotello, V. M. *Nat. Chem.* **2010**, *2*, 962.
- (c) Giljohann, D. A.; Seferos, D. S.; Daniel, W. L.; Massich, M. D.; Patel, P. C.; Mirkin, C. A. *Angew. Chem., Int. Ed.* **2010**, *49*, 3280.
- (d) Dhar, S.; Daniel, W. L.; Giljohann, D. A.; Mirkin, C. A.; Lippard, S. J. *J. Am. Chem. Soc.* **2009**, *131*, 14652.
- (3) (a) Lim, D.-K.; Jeon, K.-S.; Hwang, J.-H.; Kim, H.; Kwon, S.; Suh, Y. D.; Nam, J.-M. *Nat. Nanotechnol.* **2011**, *6*, 452. (b) Kucska, G.; Maurer, P. C.; Yao, N. Y.; Kubo, M.; Noh, H. J.; Lo, P. K.; Park, H.; Lukin, M. D. *Nature* **2013**, *500*, 54. (c) Lee, J.-S.; Han, M. S.; Mirkin, C. A. *Angew. Chem., Int. Ed.* **2007**, *46*, 4093. (d) de la Rica, R.; Stevens, M. M. *Nat. Nanotechnol.* **2012**, *7*, 821.
- (4) (a) Turner, M.; Golovko, V. B.; Vaughan, O. P. H.; Abdulkhan, P.; Berenguer-Murcia, A.; Tikhov, M. S.; Johnson, B. F. G.; Lambert, R. M. *Nature* **2008**, *454*, 981. (b) Grirrane, A.; Corma, A.; García, H. *Science* **2008**, *322*, 1661. (c) Gross, E.; Liu, J. H.-C.; Toste, F. D.; Somorjai, G. A. *Nat. Chem.* **2012**, *4*, 947.
- (5) (a) Zhou, W.; Dridi, M.; Suh, J. Y.; Kim, C. H.; Co, D. T.; Wasielewski, M. R.; Schatz, G. C.; Odom, T. W. *Nat. Nanotechnol.* **2013**, *8*, 506. (b) Chen, A. Y.; Deng, Z.; Billings, A. N.; Seker, U. O. S.; Lu, M. Y.; Citorik, R. J.; Zakeri, B.; Lu, T. K. *Nat. Mater.* **2014**, *13*, 515.
- (c) Rosi, N. L.; Giljohann, D. A.; Thaxton, C. S.; Lytton-Jean, A. K. R.; Han, M. S.; Mirkin, C. A. *Science* **2006**, *312*, 1027. (d) Liu, J.; Yu, M.; Zhou, C.; Yang, S.; Ning, X.; Zheng, J. *J. Am. Chem. Soc.* **2013**, *135*, 4978.
- (6) (a) Yang, P.; Xu, Q.-Z.; Jin, S.-Y.; Zhao, Y.; Lu, Y.; Xu, X.-W.; Yu, S.-H. *Chem. - Eur. J.* **2012**, *18*, 1154. (b) Morandi, V.; Marabelli, F.; Amendola, V.; Meneghetti, M.; Comoretto, D. *Adv. Funct. Mater.* **2007**, *17*, 2779.

- (7) (a) Kamata, K.; Lu, Y.; Xia, Y. *J. Am. Chem. Soc.* **2003**, *125*, 2384.  
(b) Lee, J.-H.; Mahmoud, M. A.; Sitterle, V.; Sitterle, J.; Meredith, J. C. *J. Am. Chem. Soc.* **2009**, *131*, 5048.
- (8) Sun, Z.; Bao, Z.; Fang, C.; Wang, J. *Langmuir* **2012**, *28*, 9082.
- (9) Liu, Y.; Li, M.; Chen, G. *J. Mater. Chem. A* **2013**, *1*, 930.
- (10) Wang, S.; Zhang, J.; Yuan, P.; Sun, Q.; Jia, Y.; Yan, W.; Chen, Z.; Xu, Q. *J. Mater. Sci.* **2015**, *50*, 1323.
- (11) Zhao, J.; Niu, W.; Zhang, L.; Cai, H.; Han, M.; Yuan, Y.; Majeed, S.; Anjum, S.; Xu, G. *Macromolecules* **2013**, *46*, 140.
- (12) Pal, B.; Sen, P. K.; Gupta, K. K. S. *J. Phys. Org. Chem.* **2001**, *14*, 284.
- (13) Noguez, C. *J. Phys. Chem. C* **2007**, *111*, 3806.
- (14) Liu, J.; Wickramaratne, N. P.; Qiao, S. Z.; Jaroniec, M. *Nat. Mater.* **2015**, *14*, 763.
- (15) Ferrari, A. C.; Rodil, S. E.; Robertson. *Phys. Rev. B: Condens. Matter Mater. Phys.* **2003**, *67*, 155306.
- (16) Sun, X.; Li, Y. *Angew. Chem., Int. Ed.* **2004**, *43*, 597.